Journal of Marine Research, 43, 13–36, 1985

Three-dimensional shelf circulation along an eastern ocean boundary

by Julian P. McCreary, Jr.[1] and Shenn-Yu Chao[1]

ABSTRACT

A linear, three-dimensional, continuously stratified model is used to study wind-driven ocean circulation near an eastern coast in the presence of a continental shelf. A simplifying assumption is that the alongshore flow field is in geostrophic balance. This assumption allows steady solutions to be obtained numerically with a very efficient scheme. As a result, it is possible to find solutions for a wide variety of model parameters and shelf profiles.

A band of equatorward wind forces the ocean, and the resulting solutions have many features in common with observations at eastern boundaries. They all have a surface equatorward jet, but do not always have a coastal undercurrent. When the shelf depth is sufficiently shallow or vertical mixing is sufficiently strong, the speed of the undercurrent, if it exists, is usually weak; in that case, only when there is positive wind curl near the coast does its speed reach commonly observed values.

Solutions are sensitive to the choice of bottom topographic profile. A general result is that the continental shelf always acts to strengthen the equatorward jet and to weaken or eliminate the undercurrent. The reason is that the shelf induces an equatorward barotropic component to the shelf currents, a component that is not present in flat-bottom solutions.

1. Introduction

An equatorward wind along an eastern ocean boundary drives an offshore Ekman drift at the ocean surface and a return flow underneath. Accompanying this upwelling cell are a surface equatorward jet and a poleward coastal undercurrent that decay offshore with a scale of the order of 20–30 km. Both the transverse, upwelling circulation and the alongshore currents are surface-trapped features which do not extend to the ocean bottom. For example, the coastal undercurrent is typically located along the continental slope at a depth of only 100–200 m. Isopycnals bend sharply upward toward the coast above the core of the undercurrent, indicating the occurrence of upwelling. They bow downward beneath the core, indicating that the upwelling is confined very near to the surface. Detailed descriptions of the pertinent observations can be found in Mooers *et al.* (1976), Kundu and Allen (1976), Hickey (1979) and Brockmann *et al.* (1980). Various aspects of coastal dynamics are reviewed by O'Brien *et al.* (1977), Allen (1980) and Huthnance (1981).

1. Nova University Oceanographic Center, 8000 North Ocean Drive, Dania, Florida, 33004, U.S.A.

a. Theoretical background. Early theoretical studies of coastal circulation completely ignore alongshore variations of the wind and the currents, and thereby reduce the problem to a two-dimensional one. Although based on the seemingly reasonable assumption that the alongshore scale of the currents is much larger than their offshore scale, the steady solutions of two-dimensional models have several major limitations. First, they generate coastal circulations that are not surface-trapped, but that extend throughout the water column. Second, for realistic values of vertical mixing alongshore currents are always unrealistically large (McCreary, 1981). Finally, they do not develop a coastal undercurrent; all currents flow in the direction of the wind.

Three-dimensional models differ fundamentally from two-dimensional ones in that they allow an alongshore pressure gradient field to develop. Consider the sudden application of an equatorward wind of finite meridional extent, that is, a wind band. Initially, the model responds just like a two-dimensional one. Then, coastally trapped waves propagate across the wind band in a time scale of the order of tens of days and establish an alongshore pressure gradient field. It is the development of this field that traps the coastal circulation near the ocean surface, limits the speed of the alongshore currents, and provides a force to drive an undercurrent (McCreary, 1981; Wang, 1982; Suginohara, 1982). On a longer time scale, a portion of the coastally trapped circulation leaks offshore because of the westward radiation of Rossby waves, weakening the surface equatorward jet and strengthening the coastal undercurrent (McCreary, 1981; Philander and Yoon, 1982; Suginohara and Kitamura, 1984; also see the discussion of Figure 7).

Mixing of heat and momentum is also an essential part of the dynamics of three-dimensional coastal models. This is apparent in that inviscid solutions are very unrealistic. For example, flat-bottom, inviscid models that include the β-effect produce no coastal currents at all! In these models the wind is introduced as a body force in a surface mixed layer. *All* of the coastal circulation propagates offshore via the radiation of Rossby waves, and the coastal ocean is left in a state of Sverdrup balance in which all flow is contained in the mixed layer. Provided the wind has no curl, this balance is a state of no motion where forcing by the wind is completely balanced by the alongshore pressure gradient field (Anderson and Gill, 1975; McCreary, 1981). The same adjustment occurs for inviscid models with bottom topography, provided that the mixed layer does not extend to the ocean bottom (Anderson and Killworth, 1977; Miura and Suginohara, 1980). It also occurs for the system of equations, (1), that we study in this paper.

McCreary (1981) discusses the sensitivity of his flat-bottom solutions to both vertical and horizontal mixing. Vertical mixing affects both the speed and structure of the alongshore currents. As vertical mixing decreases, the equatorward jet and undercurrent strengthen, and they are increasingly surface trapped. Horizontal mixing weakens the alongshore currents by diffusing them offshore, but does not significantly change their vertical structure. In barotropic models, bottom drag plays an important

role. For example, the coastal current in the barotropic model of Csanady (1978) owes its existence to the presence of bottom drag, and its speed is inversely proportional to the drag coefficient. In continuously stratified models, however, bottom drag retards the currents near the ocean bottom, but otherwise does not much influence the flow (Suginohara and Kitamura, 1984; see the discussion of Figure 6).

At the present time there are only a few three-dimensional, continuously stratified, coastal models that include a continental shelf. The reason for this lack is that solutions are difficult to obtain. It is generally not possible to find solutions analytically. Moreover, numerical models require a large number of levels (or layers) in order to resolve the vertical structure of the flow field, thereby making integrations very costly. Two pioneering studies are the numerical models of Wang (1982) and of Suginohara (1982). Both models generate a realistic coastal flow field, including a weak undercurrent, and they illustrate the role of shelf waves in the establishment of the coastal circulation. Both, however, are limited in that they are integrated for only a short period of time (less than 20 days), a time insufficient for solutions to approach equilibrium.

Recently, Suginohara and Kitamura (1984) extended the Suginohara (1982) calculation by integrating the model for 210 days, and they compared solutions with and without the β-effect. Without β, the initial undercurrent (formed during the first 20 days) weakened and eventually disappeared. With β, the initial undercurrent strengthened somewhat and shallowed. The authors demonstrated that the difference in these two calculations was due to the offshore spreading of the coastal currents caused by the β-effect.

Suginohara and Kitamura's quasi-steady solutions have two interesting features that contrast markedly with the steady, flat-bottom solutions of McCreary (1981). First, the maximum speed of the undercurrent is very weak even at day 200, never being greater than 2 cm/sec. Second, the depth-averaged alongshore flow is never zero, so that the currents over the shelf always have a barotropic component. In the flat-bottom solutions of McCreary (1981), on the other hand, the undercurrent speed reaches 30 cm/sec or more, and there is no barotropic component to the flow.

b. The present approach. This paper continues the effort to model the three-dimensional circulation near an eastern ocean boundary in the presence of a continental shelf. The model is linear, continuously stratified and viscid. There is vertical and horizontal mixing of heat and momentum and also bottom drag. Wind stress enters the ocean as a body force spread throughout a surface layer. The continental shelf is assumed to be independent of the alongshore coordinate, but otherwise can have an arbitrary shape. Finally, the alongshore velocity field is assumed to be in geostrophic balance. This assumption allows only poleward-decaying waves in the system (see the discussion in section 2a), and greatly facilitates the numerical solution of the equations of motion.

Solutions are not found in the usual way by stepping the fields forward in time at each grid point until a steady state is reached. Instead, all time-derivatives are dropped from the equations of motion, and steady-state solutions are found directly. They are found by solving for the pressure field everywhere in a transverse section, and then by stepping the field poleward in space. Physically, the reason for the success of this procedure is that the alongshore stepping occurs in the direction of decay of the possible waves of the system. Mathematically, the reason is that the assumption of alongshore geostrophy reduces the order of the y-derivatives that appear in the equation for pressure. Since time is eliminated as a variable, the scheme is computationally very efficient.

The model is similar to two previous ones. It can be regarded as a generalization of the homogeneous model of Csanady (1978) that includes stratification, and as an extension of the flat-bottom model of McCreary (1981) that allows for a continental shelf. Both of these earlier studies assume alongshore geostrophy, and represent solutions analytically in terms of an alongshore integral, a procedure that is essentially the same as the one used here.

Because the model is computationally so efficient, it is possible to find and compare solutions for a variety of parameter values and bottom topographic profiles. Solutions are particularly sensitive to the strength of vertical mixing and to the depth of the shelf at the coast. For sufficiently strong mixing or shallow shelf depths, the undercurrent is weak or absent; in that event, only when the wind has positive curl does its speed increase to commonly observed values.

2. The model ocean

a. Equations of motion. In a state of no motion the model ocean has a stably stratified background density structure $\rho_b(z)$ and associated Väisälä frequency $N_b(z)$. Assuming that the alongshore flow field is in geostrophic balance, the steady-state equations of motion linearized about the background state are

$$fu + p_y = G(x, y, z) + \nu v_{zz} + \nu_h v_{xx}, \quad -fv + p_x = 0,$$
$$-\frac{1}{g} N_b^2 w = \kappa \rho_{zz} + \kappa_h \rho_{xx}, \quad p_z = -\rho g, \quad u_x + v_y + w_z = 0, \tag{1}$$

where ν and κ are coefficients of vertical eddy viscosity and diffusivity respectively, and ν_h and κ_h are coefficients of horizontal eddy viscosity and diffusivity. For simplicity we take $\nu = \kappa$ and $\nu_h = \kappa_h$. The zonal, meridional and vertical velocity fields are u, v and w, respectively; p and ρ are the pressure and density changes from the background state; f is the Coriolis parameter; g is the acceleration due to gravity. The x-axis is oriented eastward, the y-axis is northward with its origin at the equator, and the z-axis is vertically upward. The meridional wind field is represented by a body force, $G(x, y, z)$, that decays rapidly with depth; the integral of $G(x, y, z)$ over the water column gives the wind stress, $\tau(x, y)$, applied at the ocean surface. The wind field is assumed to be

nonzero only in a region of finite meridional extent that does not extend to the equator.

It is possible to derive from (1) a single equation in p alone

$$\frac{\nu_h}{f}p_{xxxx} + \frac{\nu}{f}p_{zzxx} + f\nu_h\left(\frac{p_{xxz}}{N_b^2}\right)_z + f\nu\left(\frac{p_{zzz}}{N_b^2}\right)_z - \frac{\beta}{f}p_x = G_x. \tag{2}$$

Because (2) involves fourth-order derivatives, it is computationally useful to define a new variable, ϕ, and to separate (2) into two coupled second-order equations

$$\begin{aligned} \nu p_{zz} + \nu_h p_{xx} &= \phi, \\ f^2(\phi_z/N_b^2)_z + \phi_{xx} &= \beta p_x - fG_x. \end{aligned} \tag{3a}$$

Rewriting the first four of Eqs. (1) in terms of p and ϕ gives

$$u = \frac{1}{f}\left[G - p_y + \frac{1}{f}\phi_x\right], \qquad v = p_x/f, \qquad w = \phi_z/N_b^2, \qquad \rho = -p_z/g. \tag{3b}$$

Eqs. (3a) are the set of equations that are solved numerically in this paper for the unknowns p and ϕ. Eqs. (3b) then give u, v, w and ρ in terms of p and ϕ.

The differential operator in (2), subject to the boundary conditions discussed next, defines a discrete set of eigenfunctions. At several points in this paper we refer to these eigenfunctions as coastal waves or as modes. Mathematically, they are closely related to the coastal waves in a time-dependent, inviscid model. Their essential difference is that they decay, rather than propagate, in the alongshore direction.

Note that (2) does not involve any y-derivatives. This lack is due entirely to the assumption that the alongshore flow is in geostrophic balance. If this assumption is not made, there are additional terms in this equation that involve second-order y-derivatives. In a time-dependent, inviscid model the neglect of these terms filters all waves with equatorward group velocity out of the system (Gill and Schumann, 1974). Similarly, in this steady, viscid model their neglect filters out all equatorward-decaying (poleward-growing) waves.

b. Boundary conditions. The model ocean is bounded by a surface at $z = 0$, a vertical wall at $x = 0$, and by variable bottom topography at $z = -h(x)$. At the sea surface, a no-stress condition and a rigid lid are adopted, so that

$$\nu v_z = w = 0. \tag{4a}$$

The no-stress condition is sensible because the effect of forcing by the wind is taken up entirely in the body force, $G(x, y, z)$. At the ocean bottom, stress has the form of bottom drag and there can be no flow normal to the bottom. Boundary conditions there are

$$\nu v_z = \gamma v, \qquad w = -u\,h_x, \tag{4b}$$

where γ is a linear drag coefficient. At the coast, a slip condition is adopted for v and there can be no flow into the wall, so that

$$v_x = u = 0. \tag{4c}$$

Another requirement is that the coastal solution vanishes far offshore, that is, as $x \to -\infty$. A final condition is that the coastal solution vanishes everywhere equatorward of the wind patch. As discussed in the Introduction, coastal models adjust to equilibrium with the wind by radiating coastally trapped waves. The reason for imposing this last condition is that all coastally trapped waves in the present system propagate poleward; hence, there is no mechanism in the model for generating any circulation equatorward of the wind band.

With the assumption of alongshore geostrophy, a boundary condition poleward of the wind band is neither necessary nor even possible. This property is also due to the fact that no second-order y-derivatives appear in Eqs. (2) or (3a). Only a first-order y-derivative appears in (3b), so that the equations of motion have a parabolic, rather than elliptic, character.

The assumption of alongshore geostrophy and the surface boundary condition, $v_z = 0$, requires that $\rho = 0$ at the ocean surface, and so the model cannot generate any sea-surface temperature variations. This property is unfortunate since an important aspect of the observed response of the coastal ocean to an equatorward wind is the appearance of cold upwelled water at the ocean surface. Nevertheless, this condition is mathematically so convenient that it has been commonly used (Allen, 1973; Pedlosky, 1974; McCreary, 1981). Moreover, it is generally accepted that the presence of an upwelling front at the ocean surface acts to modify, not to destroy, the model response under the idealized condition (4a).

In terms of p and ϕ, boundary conditions (4) can be rewritten as follows. At the ocean surface,

$$p_z = \phi_z = 0. \tag{5a}$$

At the ocean bottom,

$$\nu p_{xz} = \gamma p_x, \qquad \frac{\phi_z}{N_b^2} = -\frac{h_x}{f}\left[-p_y + \frac{1}{f}\phi_x + G\right]. \tag{5b}$$

At the coast,

$$p_y = \frac{1}{f}\phi_x + G, \qquad \phi = \nu p_{zz}. \tag{5c}$$

The numerical method requires an artificial offshore boundary at $x = -L$. Boundary conditions imposed there are

$$p_x = \phi_x = 0. \tag{5d}$$

Finally, at the equatorward edge of the wind patch it is sufficient to require

$$p = 0. \tag{5e}$$

c. The numerical method. It is convenient to solve (3a), subject to boundary conditions (5), in a rectangular domain. Therefore, the independent variables (x, z) are transformed to a stretched coordinate system (x', θ) according to

$$x' = x, \qquad \theta = z/h(x). \tag{6}$$

(Wang and Mooers, 1976, and others have also utilized this transformation.) One advantage of this new coordinate system is that it allows the shelf structure to be easily changed in the numerical code. Another is that it allows p and ϕ to be very well resolved vertically in the nearshore region where $h(x)$ is small. The governing equations and boundary conditions, expressed in the stretched coordinates, are written down in Appendix A.

Solutions are evaluated on a grid in the region shown in Figure 1 from $x = -L$ to 0, from $z = -h(x)$ to 0 and from 20N to 60N. Most of the solutions shown here have $L =$ 30 km, the sole exception being for the solutions of Figure 8. Grid points are located on a rectangular lattice separated by the distances $\Delta x' = 1$ km, $\Delta\theta = .0333$ and $\Delta y =$ 22.2 km, so that there are $N_x = 31$ grid points offshore and 200 grid points alongshore. It is necessary to store fields at a set of grid points just beneath the ocean bottom; so, there are $N_\theta = 32$ grid points vertically. Values of both p and ϕ are associated with each grid point.

The equations of motion (A3) and the boundary conditions (A4) are written down in a standard finite-difference form. Nearly all derivatives are center differenced, and only involve values at nearest-neighbor grid points, the sole exceptions occurring in some of the expressions for the boundary conditions. The y-derivatives of the pressure field in boundary conditions (A4b) and (A4c) are lagged in space. More precisely, the finite-difference form of p_y at point P is $(p_P - p_S)/\Delta y$, where the subscript S indicates the first grid point south of point P. Details of the finite-difference formulation are discussed in Appendix B.

In finite-difference form, then, the system reduces to a coupled set of simultaneous linear equations. There are two equations associated with each grid point, and so the total number of equations in a transverse section is $a = 2\,N_xN_\theta = 1984$. This set can be summarized in the matrix form

$$A\,Q = B, \tag{7}$$

where A is a matrix of dimension a that consists of the coefficients of the finite-difference equations, the solution Q is a column vector of the values of p and ϕ at each grid point in the transverse section, and B is a column vector of the forcing. It is useful to order the grid points, and also the equations corresponding to them, so that point 1 is

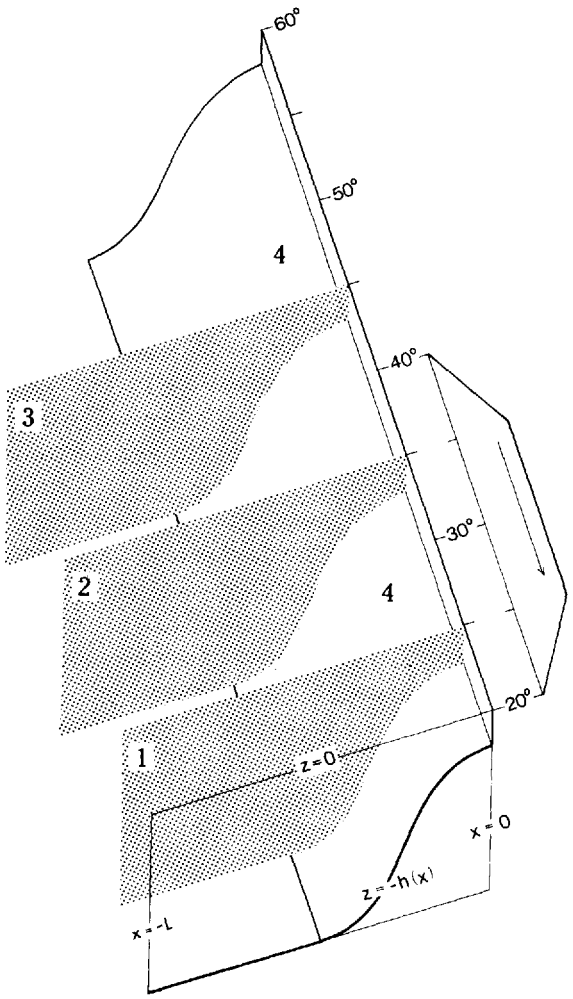

Figure 1. A schematic diagram of the model geometry showing the locations of sections 1–4, the position of the coast, and the structure of the wind band. The thick curve indicates the bottom topographic profile, $h(x)$. For most solutions $L = 30$ km. The meridional profile of the wind is indicated on the right. The equatorward wind is either zonally uniform, or increases offshore at a rate of 0.5 dyn/cm^2 per 100 km within 30 km distance of the coast. The coastal wind stress reaches a maximum of 0.5 dyn/cm^2. The structure of the wind field is described more precisely in Eqs. (8)–(11).

at the bottom-west corner of the section, point N_θ is at the top-west corner, point $N_\theta + 1$ is immediately to the east of point 1, and so on. In that case, matrix A has a bandwidth of the order of $b = 2N_\theta = 64$, a value much smaller than a.

Eq. (7) is solved exactly using the standard technique of Gaussian elimination by "LU decomposition" (Forsythe and Moler, 1967). [Attempts at using an iterative

scheme (successive over-relaxation) to solve the system generally failed. This failure was due to the fact that the matrix is not diagonally dominant.] Because A is sufficiently nonsingular, pivoting is not necessary. For a general matrix, A, the solution of (7) on a computer using this method requires roughly a^2 words of storage and $a^3/3$ multiplications, both excessively large numbers. When A is ordered as above, the solution requires only $2ab$ words of storage and ab^2 multiplications.

The solution proceeds by solving for the pressure field at all grid points in a particular transverse section, and then advancing poleward a distance Δy to find the pressure field in the next transverse section, and so on. This method makes good sense physically, because the direction of y-stepping is poleward, and so automatically builds in the property that the coastal waves allowed by the system all decay poleward. (As a test, several runs were attempted when the direction of y-stepping was equatorward; not surprisingly, the solutions all became unbounded after several steps.) Thus, the method is quite similar to that used in an ordinary implicit, time-stepping model where the solution at every grid point is advanced in time by an increment Δt, except that in this case the alongshore coordinate replaces time.

3. Results

The model was used to study the response of the ocean to an equatorward wind forcing,

$$G(x, y, z) = \tau_o X(x)\, Y(y)\, Z(z), \tag{8}$$

where $\tau_o = -0.5$ dyn/cm^2. The zonal profile of the wind is given by

$$X(x) = \begin{cases} 1 - cx, & 0 \geq x > x_c, \\ 1 - cx_c, & x \leq x_c, \end{cases} \tag{9}$$

where $x_c = -30$ km. The majority of the solutions in this paper are driven by a zonally uniform wind, so that $c = 0$ in (9), the sole exception being for the solutions in Figure 9. The latitudinal variation of the wind is given by

$$Y(y) = \begin{cases} (y - y_o)/\delta & y_o \leq y < y_o + \delta \\ 1, & y_o + \delta \leq y < y_o + 3\delta, \\ -(y - y_o - 4\delta)/\delta, & y_o + 3\delta \leq y < y_o + 4\delta, \\ 0, & \text{otherwise}, \end{cases} \tag{10}$$

where $\delta = 5° \times (\pi/180°) \times R$, $y_o = 20° \times (\pi/180°) \times R$, and R is the radius of the earth. This meridional profile is chosen to resemble the steady component of the winds off the western coast of North America (Nelson, 1976), and is shown in Figure 1. The wind stress projects into the upper ocean as a body force with the vertical profile

$$Z(z) = \frac{2}{\sqrt{\pi}} \frac{\sqrt{\ln 10}}{D} e^{-(\ln 10) z^2/D^2}, \tag{11}$$

which decays rapidly with depth with a ten-folding scale of D. The profile satisfies the integral relation $\int_{-\infty}^{0} Z(z)\, dz = 1$, so that the vertical integral of G yields the wind stress, $\tau(x, y)$, applied at the sea surface.

The continental shelf and slope profile is given by

$$h(x) = \begin{cases} h_o + \dfrac{h_T - h_o}{2}\left(1 - \cos\dfrac{\pi}{s}x\right), & 0 \geq x > -s, \\ h_T, & x \leq -s, \end{cases} \tag{12}$$

where h_o is the water depth at the coast, h_T the water depth at the flat-bottom ocean interior, and s is the width of the shelf and slope region. This profile is illustrated schematically by the thick curve in Figure 1.

There is no restriction on f or β in this ocean model. Unless stated otherwise,

$$f = 2\,\Omega \sin(y/R), \qquad \beta = (2\,\Omega/R)\cos(y/R), \tag{13}$$

where $\Omega = 2\,\pi$ day^{-1}. Finally, the background density structure chosen for this study is the linear profile,

$$\rho_b(z) = 1 - \Delta\rho\,\frac{z}{d}, \tag{14}$$

where $d = 500$ m, although the model poses no such restriction.

a. The coastal circulation. In this section we discuss the coastal circulation driven by a curl-free wind field, so that $c = 0$ in (9). For these solutions the ten-folding scale of the wind forcing is $D = 60$ m, the bottom topographic profile is set such that $h_o = 90$ m, $h_T = 500$ m and $s = 15$ km, and the background stratification profile has $\Delta\rho = 0.005$ g/cm^3. This choice for $\Delta\rho$ ensures that N_b^2 $(= -g\Delta\rho/\bar{\rho}d)$ has a value that is typical for the upper part of the water column in coastal upwelling regions. Values of mixing parameters are $\nu = 20$ cm^2/s, $\nu_h = 10^5$ cm^2/s and $\gamma = 0$.

The four sections shown in Figure 1 are chosen to describe the three-dimensional flow field. Sections 1–3 are sections transverse to the coast, whereas section 4 is an alongshore section coinciding with the coastal wall and the bottom boundary. Figures 2a–c show the circulation patterns and the structure of the density field on sections 1–3, respectively, and Figure 2d shows the circulation pattern along section 4. In order to display adequately the weaker poleward flows, the contour intervals for equatorward and poleward currents are different, being 5 cm/s and 2 cm/s, respectively. (The same contour intervals are also used later in Figs. 4–9.)

The alongshore flow field at lower latitudes has an equatorward surface jet and a poleward undercurrent attached to the shelf. The speed of the surface jet reaches a maximum of 64 cm/s near the northern edge of the wind band at 35N. In contrast, the speed of the coastal undercurrent increases to a maximum of only about 8 cm/s at 26N

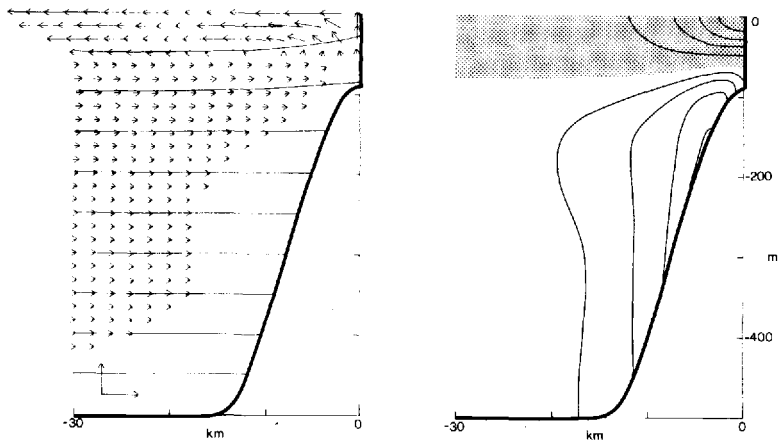

Figure 2a. Vertical sections of transverse circulation and density structure (left panel) and alongshore current (right panel) along section 1 of Figure 1. The velocity contour interval is 5 cm/sec for equatorward flow (shaded regions), but is 2 cm/sec for the weaker poleward flows. *Calibration vectors in the lower left corner of left panels are .001 cm/sec and 1 cm/sec in the* vertical and horizontal directions, respectively. The isopycnal contour interval is .0005 g/cm^3, and the uppermost isopycnal has the value 1.0005 g/cm^3.

and then decreases rapidly poleward, vanishing at about 40N. As in the Suginohara and Kitamura (1984) study, the coastal undercurrent is weak and the currents over the shelf have a strong barotropic component. Finally, equatorward flow is still strong well north of 40N, where the current is entirely remotely driven by the winds to the south.

The transverse flow field has features that compare favorably with those observed. In the region of the wind band there is an offshore surface drift of the order of 1.5 cm/s. Consequently, there is a divergence of fluid from the coast, and upwelling into the

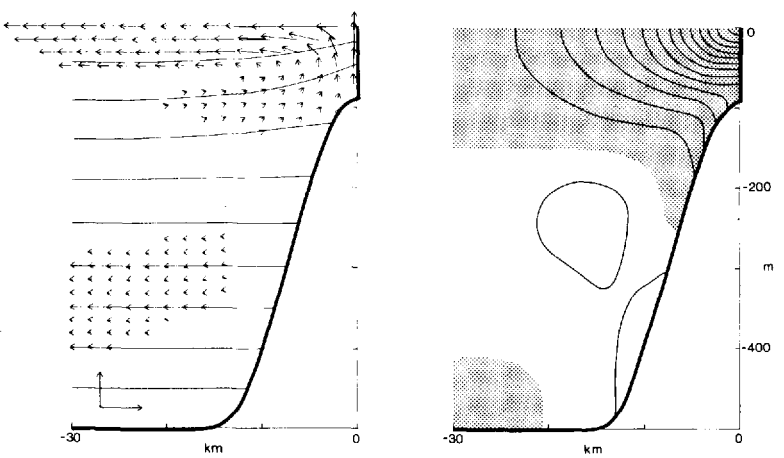

Figure 2b. As in Figure 2a, except along section 2 of Figure 1.

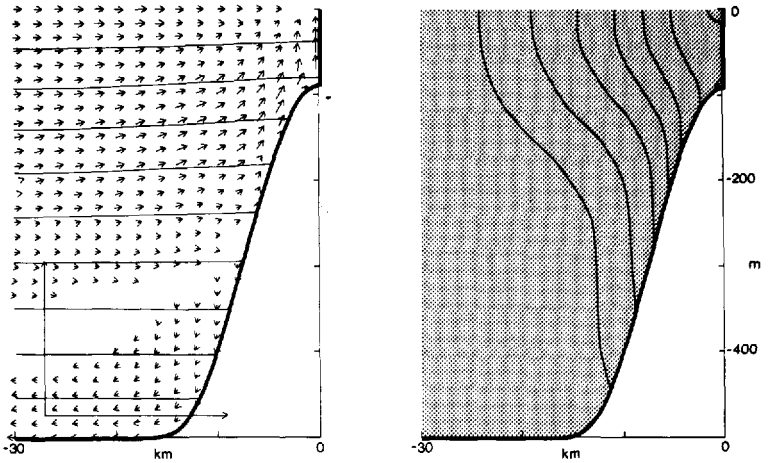

Figure 2c. As in Figure 2a, except along section 3 of Figure 1. The length of calibration arrows indicates that the transverse circulation is very weak.

surface layer occurs at speeds as large as .007 cm/s. The upwelling is confined near the ocean surface, and there is weak downwelling beneath the core of the undercurrent if one is present. The strongest onshore flow occurs nearshore just below the offshore surface drift at weak speeds of about 0.26 cm/s, and the net onshore transport is never sufficient to balance the offshore transport at the surface. In contrast to the alongshore

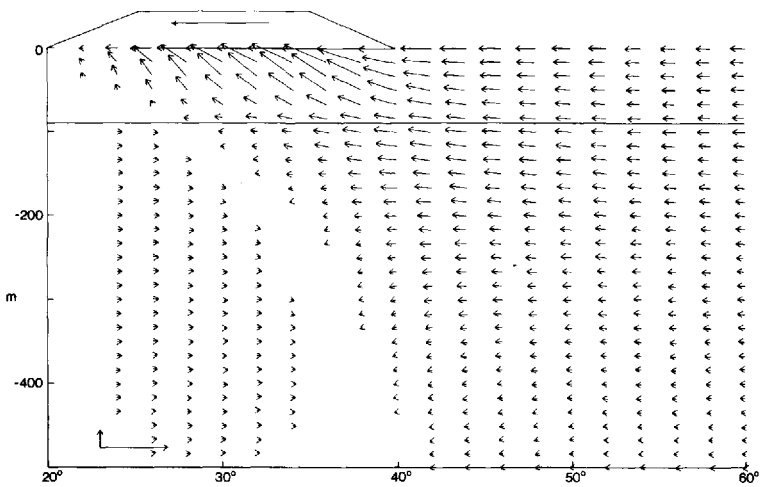

Figure 2d. Velocity field along section 4 of Figure 1. Calibration vectors in the lower left corner of the figure are .001 cm/sec and 100 cm/sec in the vertical and horizontal directions, respectively. Currents above (below) the horizontal line at $z = -90$ m are coincident with the coastal wall (shelf). The meridional profile of the wind is indicated at the top of the figure. The alongshore current extends poleward well beyond the region of the wind band, but the upwelling does not. The undercurrent does not penetrate very far poleward.

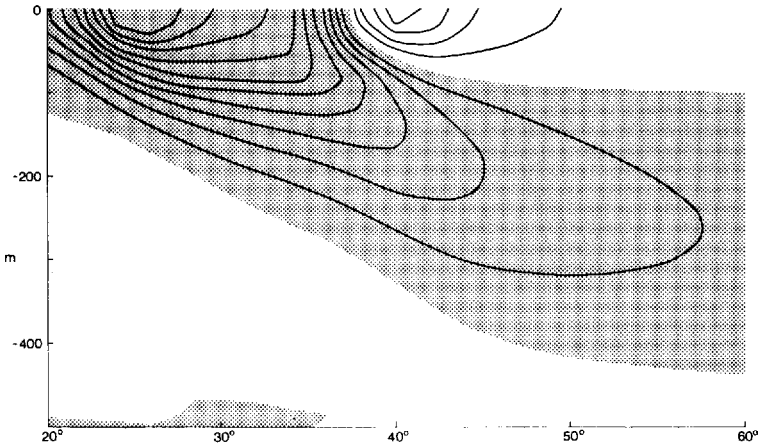

Figure 3. Alongshore pressure gradient field along section 4 of Figure 1. The contour interval is 5×10^{-6} dyn/g. The pressure gradient field decays rapidly with depth.

flow, significant transverse circulation is confined to the region of the wind band, and so is predominantly locally forced by the wind.

The density field, $\rho_b(z) + \rho(x, y, z)$, satisfies the thermal wind relationship. Isopycnals at depths less than that of the undercurrent core bend upward, and isopycnals at greater depths bend downward. North of 40N, where the coastal undercurrent is absent, the bending of isopycnals is entirely upward.

Figure 3 shows the alongshore pressure gradient p_y along section 4. The surface gradient is negative from 20N to 37N, corresponding to a northward drop in sea level of 7 cm, and is weakly positive farther poleward. The minimum pressure gradient is -6×10^{-5} dyn/g at 25N, equivalent to a sea level slope of -6×10^{-8}. The maximum surface pressure gradient is 2×10^{-5} dyn/g at about 40N, the poleward edge of the wind band. The pressure gradient decreases rapidly with depth. Slightly below the core of the undercurrent the pressure gradient changes sign, becoming weakly positive.

b. The dependence on model parameters. The model has five free parameters: ν, ν_h, γ, $\Delta\rho$ and D. It is important to know how the response of the model depends on these parameters. Figures 4–6 compare structures of alongshore currents for a range of values of ν, ν_h and γ, respectively. The model dependence on $\Delta\rho$ and D is less interesting, and so these results are discussed briefly without reference to figures.

Figure 4 shows the alongshore flow fields at section 2 when $\nu = 5$ cm^2/s and 10 cm^2/s and all other parameters remain the same as in Figure 2b. As ν weakens, the alongshore currents become stronger and shallower. In particular, the coastal undercurrent strengthens markedly, indicating that the undercurrent penetrates much farther poleward. Thus, the vertical structure of the currents is strongly influenced by ν. Indeed, whether an undercurrent exists at all can be decided by the choice of ν. As noted in the Introduction, flat-bottom solutions of McCreary (1981) exhibit a similar

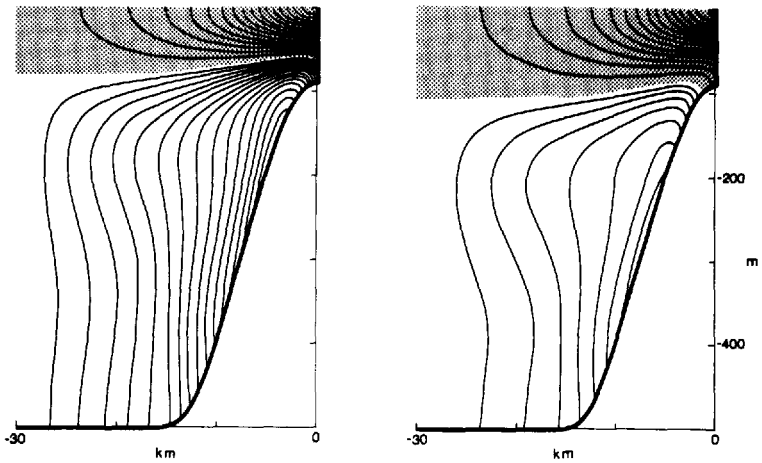

Figure 4. Vertical section of alongshore current contrasting solutions when $\nu = 5$ cm^2/s (left panel) and $\nu = 10$ cm^2/s (right panel) along section 2. The velocity contour interval is 5 cm/s for equatorward flows (shaded regions), but is 2 cm/s for the weaker poleward flows. Compare these solutions to that of Figure 2b for which $\nu = 20$ cm^2/s. As ν decreases the currents strengthen and are more surface trapped, and the undercurrent penetrates much farther poleward.

dependence on ν. The difference is that with a flat bottom there is never a barotropic component to the flow, and so the undercurrent exists for all values of ν.

Figure 5 compares alongshore flow fields at section 1 for $\nu_h = 10^4$ cm^2/s and 10^6 cm^2/s, and all other parameters are the same as in Figure 2a. The changes caused by horizontal mixing are minor, even though ν_h varies by two orders of magnitude. The most obvious change is that as ν_h increases, the alongshore currents weaken and spread farther offshore. Horizontal mixing does not significantly influence their vertical structure, and does not determine whether an undercurrent exists. A similar weak dependence occurs for the flat-bottom solutions of McCreary (1981).

Figure 6 compares solutions along section 1 in which the values of bottom friction are $\gamma = .001$ cm/s and .01 cm/s, and other parameters are unchanged. Without bottom drag (Fig. 2a), contours of the coastal undercurrent approach the bottom boundary vertically due to condition (4b). With bottom drag, the speed of currents near the bottom decreases, causing an onshore bending of the isotachs. As a result, an increase of bottom drag tends to weaken and raise the undercurrent. Figure 2b and the left panel of Figure 8 contrast solutions at section 2 with $\gamma = 0$ and $\gamma = .001$ cm/s, respectively. In this case, bottom drag has little effect on the solution; with bottom drag, the equatorward jet is somewhat weaker and the undercurrent is marginally stronger. In general, bottom drag modifies the near-bottom strength and structure of the alongshore currents, but it does not determine whether an undercurrent exists.

A decrease in the background stratification deepens the alongshore currents, strengthens the equatorward jet and weakens the undercurrent. These properties make

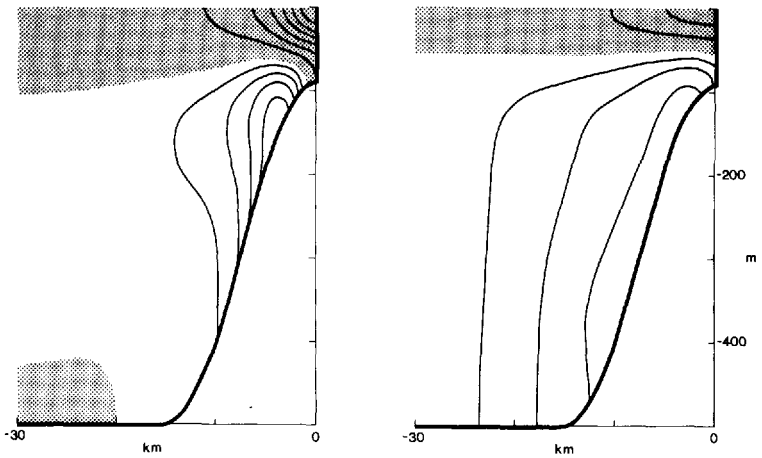

Figure 5. As in Figure 4, except contrasting solutions when $\nu_h = 10^4$ cm^2/s (left panel) and $\nu_h = 10^6$ cm^2/s (right panel) along section 1. Compare these solutions to that in Figure 2a for which $\nu_h = 10^5$ cm^2/s. Solutions are not very sensitive to changes in ν_h. Horizontal mixing acts only to diffuse the currents farther offshore.

sense, since the currents should become more barotropic as stratification weakens. The model is generally insensitive to the depth D in which the wind forcing is projected into the upper ocean. The primary effect is that as D decreases the equatorward jet and the offshore drift strengthen. The undercurrent remains largely unaffected, as long as D is smaller than the coastal ocean depth, h_o.

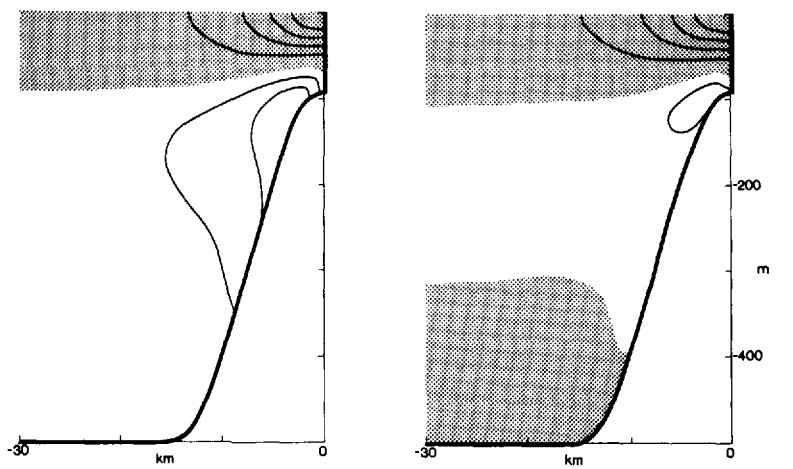

Figure 6. As in Figure 4, except contrasting solutions when $\gamma = .001$ cm/s (left panel) and $\gamma = .01$ cm/s (right panel) along section 1. Compare these solutions to that in Figure 2a for which $\gamma = 0$. Bottom drag acts to weaken currents near the ocean bottom.

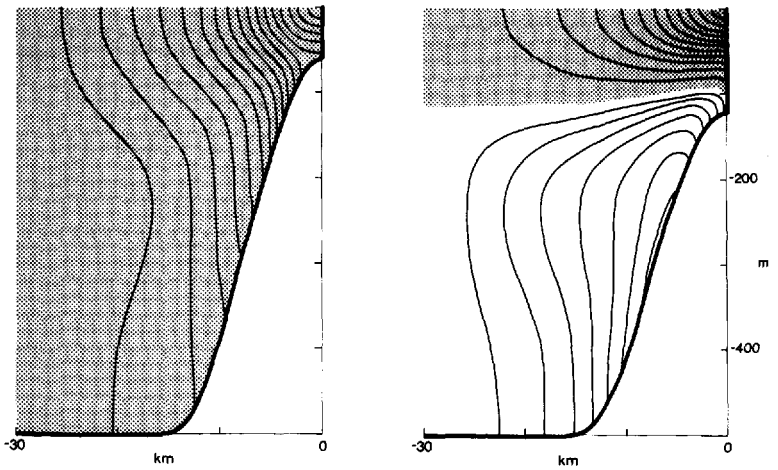

Figure 7. As in Figure 4, except contrasting solutions when h_o = 60 m (left panel) and h_o = 120 m (right panel) along section 2. Compare these solutions to that in Figure 2b for which h_o = 90 m. As h_o increases, the equatorward jet weakens, the undercurrent strengthens, and the barotropic component of the flow decreases.

c. The dependence on bottom topography. We have found solutions for a variety of bottom topographic profiles. For example, in one experiment a 5 km-wide flat shelf was added to the nearshore region, that is, the coastal wall was moved 5 km to the east. The inclusion of this inner shallow shelf weakened the coastal undercurrent over the slope significantly. In another experiment the width of the shelf was doubled, so that s = 30 km in (12). The equatorward jet was hardly affected at all by this change, but the undercurrent weakened. In a third experiment both h_T and s were doubled to 1000 m and 30 km, respectively. The nearshore flow field (at depths less than 500 m) was not significantly modified by the deeper bottom offshore.

Figure 7 compares alongshore flow fields at section 2 for two coastal depths, h_o = 60 m and 120 m, and all other parameters are the same as in Figure 2b. It is evident that as h_o increases the equatorward jet weakens, the undercurrent strengthens, and the barotropic component of the shelf flow decreases. These tendencies continue as h_o increases further. When h_o = 500 m (so that the ocean is flat) the speed of the equatorward jet decreases to 42 cm/s, the speed of the undercurrent increases to 17 cm/sec, and the barotropic component vanishes.

These results suggest the following conclusions. The strength and structure of the alongshore currents are most sensitive to the depth of the shelf at the coast. If the shelf is shallow enough, there is no undercurrent at the coast and the undercurrent over the slope is weak or absent. The presence of a shelf *always* weakens the undercurrent. This weakening does not occur because the shelf acts to weaken the baroclinic (shear) component of the flow. It occurs because the shelf induces an equatorward barotropic (depth-averaged) component that overwhelms the baroclinic part.

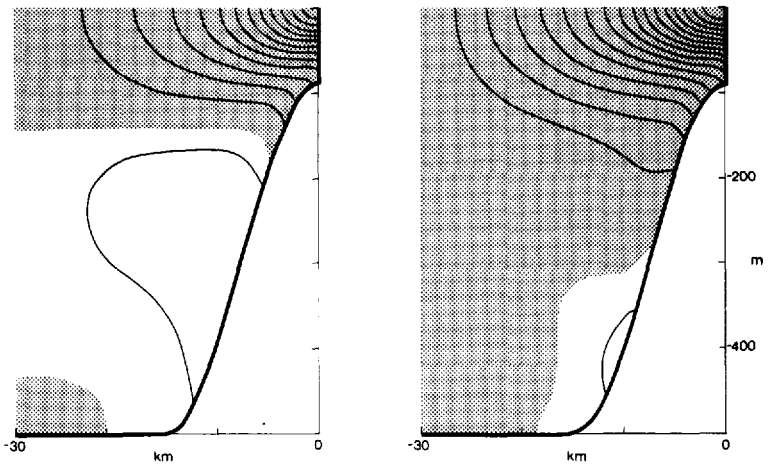

Figure 8. As in Figure 4, except contrasting solutions with β (left panel) and without β (right panel) along section 2 when $\gamma = .001$ cm/s. The β-effect weakens the equatorward jet significantly, and strengthens the undercurrent slightly.

In flat-bottom models it is easy to understand why the coastal circulation has no depth-averaged component. *All* the depth-averaged flow is associated with the barotropic mode of the system. Because this mode has a depth-independent vertical structure, it is not affected by vertical mixing; as a result, the coastal currents corresponding to this mode leak *completely* offshore due to β. It is not obvious why bottom topography modifies this flat-bottom result so markedly. A likely reason is that with bottom topography there is no single mode [i.e., eigenfunction of the operator in (2) subject to appropriate boundary conditions] that is analogous to the barotropic mode. Essentially all the modes now have some depth-averaged component (Wang and Mooers, 1976), and so not all of the depth-averaged flow can leak offshore.

d. The f-plane response. The f-plane response is found by setting $\beta = 0$ in (3a), and specifying f to have its value at $y = y_o$. Figure 8 compares solutions at section 2 with β (left panel) and without β (right panel) when $\gamma = .001$ cm/s and all other parameters are the same as in Figure 2. It is clear that β acts to weaken the equatorward flow significantly and to increase slightly the poleward undercurrent. This result is consistent with those of McCreary (1981) and of Suginohara and Kitamura (1984), and is certainly due to offshore spreading caused by β.

An f-plane experiment was also carried out without bottom drag, but did not produce a realistic flow field. The solution developed a barotropic, alongshore current that grew linearly away from the offshore boundary. Such a current is clearly not realistic, since it "feels" the presence of the artificial offshore boundary. Why did this solution develop? Let P be the integral of p over the water column. In a flat-bottom region and without bottom drag, Eqs. (3a) and conditions (5a) and (5b) imply that

$\nu_h P_{xxxx} = \beta P_x$. With β, this equation describes a Munk (1950) layer, and so barotropic disturbances generated at the offshore boundary will be confined to a narrow boundary layer there. Without β, however, the equation reduces to $P_{xxxx} = 0$. Conditions (5a), (5b) and (5d) imply that $P_x = P_{xxx} = 0$ at $x = -L$, and so it follows that a possible solution of the system is that P_x is proportional to $(x - L)$.

e. The effect of wind curl. In a flat-bottom ocean it is well-known that a positive wind curl drives a poleward Sverdrup flow. Off the California coast the wind does have positive curl, with equatorward wind increasing offshore at a rate of about .5 dyn/cm^2 per 100 km. Here we investigate the effect of this wind curl on the coastal circulation.

Figure 9 shows the structure of the alongshore currents at sections 1 and 2 when $c = 5 \times 10^{-8}$ cm^{-1} in (9) and the offshore boundary is located at $x = -45$ km. All other parameters are the same as in Figure 2, except that $\gamma = .001$ cm/s. At section 1 the equatorward jet is present only within 6 km of the coastline. The undercurrent core is shallower and stronger than that in Figure 3a, reaching a speed of about 16 cm/s. At section 2 the alongshore current is equatorward everywhere near the surface, but is weaker than that in Figure 2b. The coastal undercurrent has a speed of 11 cm/s, much stronger than that in Figure 2b. Thus, wind curl does significantly alter the coastal circulation. Positive wind curl increases poleward flow everywhere over the shelf, thereby strengthening the undercurrent.

One experiment was carried out with the offshore boundary located at $x = -30$ km, but did not produce a realistic flow field. This problem occurred because the offshore boundary was adjacent to the region of wind curl (i.e., the region $x \geq x_c = -30$ km), and the poleward current generated by the wind curl was not compatible with the offshore boundary condition, $v = 0$. We avoided this problem simply by moving the offshore boundary to $x = -45$ km.

4. Summary and discussion

This paper investigates the wind-driven response of the coastal ocean in the presence of a continental shelf. The model ocean is linear, continuously stratified, and assumes alongshore geostrophy. This latter property allows steady solutions to be found with a very efficient numerical scheme. The ocean is forced by an equatorward wind confined between 20 and 40N. For most solutions the wind has no curl. For one solution the wind has positive curl near the coast.

Solutions develop a realistic current structure. Offshore drift at the surface forces upwelling at the coast that does not extend to great depths. As a result, near-surface isopycnals slope upward toward the coast. There is always a surface equatorward jet, and sometimes a coastal undercurrent, both with a width and thickness comparable to those observed. When there is an undercurrent, there is weak downwelling beneath its core and isopycnals slope slightly downward toward the coast. The dynamic height of

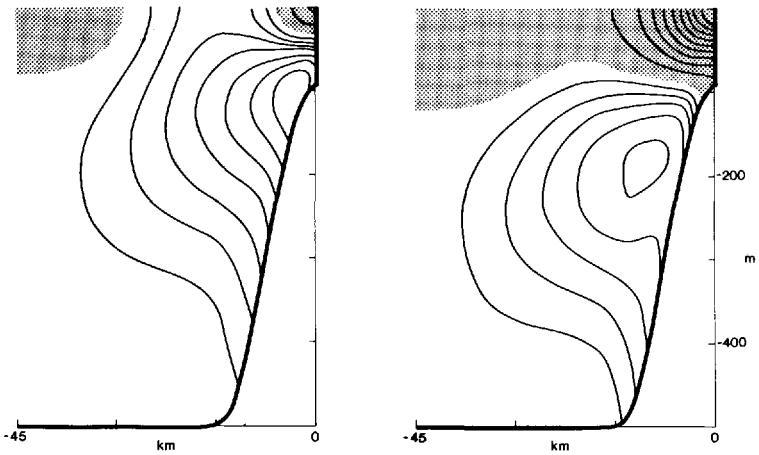

Figure 9. As in Figure 4, except showing the solutions along section 1 (left panel) and section 2 (right panel) when the ocean is forced by a wind with positive curl. The wind curl strengthens poleward flow everywhere over the shelf.

the sea surface slopes downward from 20 to 37N and then gradually increases farther poleward. The associated poleward pressure gradient field weakens markedly with depth, eventually becoming weakly equatorward.

Because the numerical scheme is so efficient it is possible to find solutions for a wide variety of model parameters. Solutions are sensitive to the amount of vertical mixing in the model. As ν decreases the alongshore currents increase in strength and are increasingly trapped to the surface, and the undercurrent penetrates much farther poleward. Horizontal mixing weakens the currents by diffusing them offshore. Bottom drag weakens near-bottom currents, but has little effect on the flow field elsewhere. As stratification weakens, the currents become more barotropic: they are less surface trapped, the equatorward jet intensifies, and the undercurrent weakens. A change in the thickness of the surface mixed layer only affects the surface currents. Similar dependencies occur in the flat-bottom solutions of McCreary (1981).

Solutions are also sensitive to the choice of bottom topographic profiles. The choice affects the strength and structure of the alongshore currents, and can even determine whether a coastal undercurrent exists. The presence of a shelf always acts to strengthen the equatorward jet and to weaken the coastal undercurrent. These changes occur because the shelf forces an equatorward barotropic component to the flow. A likely reason for the presence of this component is that with bottom topography *all* coastally trapped waves have a depth-averaged component; there is no analog to the *single* barotropic mode of a flat-bottom model.

When vertical mixing is sufficiently strong or the shelf is sufficiently shallow, the undercurrent is always weak or even absent, in agreement with the solutions of Suginohara and Kitamura (1984) but in marked contrast with the flat-bottom

solutions of McCreary (1981). In that case, only when the ocean is forced by a wind with positive curl is it possible to produce an undercurrent with a realistic speed. In a flat-bottom ocean positive wind curl forces a Sverdrup flow with a net poleward transport. A similar result holds even when there is bottom topography.

It is important to keep in mind the dynamical limitations of this model. For example, it cannot generate any sea-surface temperature variations, and hence cannot be used to study the nearshore coastal upwelling front. The nonlinear terms are ignored everywhere, and they are not always small. Finally, the assumption of alongshore geostrophy prohibits us from investigating the effects of small-scale bottom topographic features in the alongshore direction, like capes or canyons. Nevertheless, because the model is so extremely economical in terms of the computer costs, we regard it as a potentially very useful tool for studying three-dimensional coastal circulation. We are currently planning to use the model to study several other problems. For example, it has been generalized to include a wind forcing that is periodic in time, and we are now studying the seasonal variations of coastal circulation along an eastern ocean boundary.

Acknowledgments. This research was supported by the National Science Foundation under Grant No. OCE-82-00431. The computation time was provided by the National Center for Atmospheric Research, which is sponsored by the National Science Foundation. Pijush Kundu suggested several improvements of an earlier version of this manuscript. We thank Linda Smith and Kevin Kohler for their programming help, and Kathy Maxson for drafting the figures.

APPENDIX A: STRETCHED COORDINATES

Under the coordinate transformation, (6), partial derivatives with respect to x and z are replaced by the operators

$$\partial_x = \partial_{x'} - \frac{h_x}{h}\theta\partial_\theta = \frac{1}{h}(\partial_{x'}h - h_x\partial_\theta\theta), \qquad \partial_z = \frac{1}{h}\partial_\theta. \tag{A1}$$

The second partial derivative with respect to x can be expressed in several different ways. The one used here is

$$\partial_{xx} = \frac{1}{h}(\partial_{x'}h - h_x\partial_\theta\theta)\left(\partial_{x'} - \frac{h_x}{h}\theta\partial_\theta\right). \tag{A2}$$

For convenience the prime is dropped from x' in the following equations.

With the replacements (A1) and (A2), Eqs. (3a) become

$$\frac{\nu}{h^2}p_{\theta\theta} + \frac{\nu_h}{h}\left[(hp_x)_x - (h_x\theta p_\theta)_x - h_x(\theta p_x)_\theta + \frac{h_x^2}{h}(\theta^2 p_\theta)_\theta\right] = \phi, \qquad \frac{f^2}{h^2}\left(\frac{\phi_\theta}{N_b^2}\right)_\theta + \frac{1}{h}$$
$$\cdot\left[(h\phi_x)_x - (h_x\theta\phi_\theta)_x - h_x(\theta\phi_x)_\theta + \frac{h_x^2}{h}(\theta^2\phi_\theta)_\theta\right] = \frac{\beta}{h}[(hp)_x - h_x(\theta p)_\theta] - fG_x. \tag{A3}$$

Boundary conditions (5a)–(5e) become the following. At the ocean surface, $\theta = 0$,

$$p_\theta = \phi_\theta = 0. \tag{A4a}$$

At the ocean bottom, $\theta = -1$,

$$\frac{\nu}{h}\left(p_{\theta x} - \frac{h_x}{h}p_\theta + \frac{h_x}{h}p_{\theta\theta}\right) = \gamma\left(p_x + \frac{h_x}{h}p_\theta\right),$$

$$\frac{1}{N_b^2 h}\phi_\theta = -\frac{h_x}{f}\left(-p_y + \frac{1}{f}\phi_x + \frac{1}{f}\frac{h_x}{h}\phi_\theta + G\right). \tag{A4b}$$

At the coast, $x = 0$, with the assumption that $h_x = 0$ there,

$$p_y = \frac{1}{f}\phi_x + G, \qquad \phi = \frac{\nu}{h^2}p_{\theta\theta}. \tag{A4c}$$

At locations far offshore the ocean bottom is assumed to be flat, and so

$$p_x = \phi_x = 0. \tag{A4d}$$

Finally, the condition

$$p = 0 \tag{A4e}$$

is applied equatorward of the wind.

APPENDIX B: FINITE-DIFFERENCE FORMULATION

Eqs. (A3) are the two equations which apply at each interior grid point. They are expressed in the usual centered-difference form that involves only nearest-neighbor points. For example, at point P the term $(hp_x)_x$ is written

$$\frac{1}{\Delta x}\left(\frac{h_E + h_P}{2}\frac{p_E - p_P}{\Delta x} - \frac{h_W + h_P}{2}\frac{p_P - p_W}{\Delta x}\right), \tag{B1}$$

and the term $(\theta p_x)_\theta$ becomes

$$\frac{1}{2\Delta\theta}\left(\theta_A\frac{p_{AE} - p_{AW}}{2\Delta x} - \theta_B\frac{p_{BE} - p_{BW}}{2\Delta x}\right), \tag{B2}$$

where subscripts indicate the direction of nearest-neighbor grid points from P, with A directly above, B directly below, AE diagonally above and to the east, and so on.

Eqs. (A3), modified by boundary conditions (A4a), apply at each grid point on the ocean surface. Eqs. (A3) require that p and ϕ are known at points just above the grid. With the aid of (A4a), these points are eliminated from Eqs. (A3) by making the replacements $p_A = p_B$, $\phi_A = \phi_B$, $p_{AE} = p_{BE}$, and so on.

The second of Eqs. (A3) is one of the equations that applies at each bottom grid point. This equation requires that ϕ is known at points just beneath the grid, and a set

of exterior grid points are defined in order to store these values. The term $(\theta p)_\theta$ is written in a manner that does not require knowledge of p beneath the bottom,

$$\frac{-\theta_{AA} p_{AA} + 4\theta_A p_A - 3\theta_P p_P}{2\Delta\theta}, \tag{B3}$$

where the subscript AA indicates the second nearest neighbor above P.

The first of Eqs. (A4b) is the other equation that holds at bottom grid points. Derivatives with respect to θ are all expressed in a way that does not require knowledge of p beneath the bottom. For example, the term $p_{\theta\theta}$ becomes

$$\frac{p_{AA} - 2p_A + p_P}{\Delta\theta^2}. \tag{B4}$$

In order to keep the band width of matrix A as small as possible, the term $p_{\theta x}$ is written

$$\frac{1}{\Delta x}\left[\frac{-p_{BE} + 4p_{AE} - 3p_E}{2\Delta\theta} - \frac{-p_{AAW} + 4p_{AW} - 3p_W}{2\Delta\theta}\right]. \tag{B5}$$

The value of p_{BE} must be p_{AAE}, and this equivalence is ensured by (B7).

The second of Eqs. (A4b) is one of the equations that holds at grid points beneath the ocean bottom. This condition essentially specifies the value of ϕ on these exterior points. In finite-difference form (A4b) becomes

$$\phi_p - \phi_{AA} - \frac{q}{r}\phi_{AE} + \frac{q}{r}\phi_{AW} + \frac{q}{r}\frac{2\Delta x f}{\Delta y} p_A = \frac{q}{r}\frac{2\Delta x f}{\Delta y}(p_{SA} + G\Delta y), \tag{B6}$$

where $q = N_b^2 h h_x \Delta\theta/(f^2\Delta x)$, $r = 1 + N_b^2 h_x^2/f^2$, and p_{SA} indicates the value of p just equatorward (south) of A. The other equation at exterior points is

$$p_P = p_{AAA}. \tag{B7}$$

This equation has no physical significance, but only serves to ensure that $p_{BE} = p_{AAE}$ in (B5).

Eqs. (A4c) apply at all coastal grid points except the surface and bottom corner points. In order to keep the bandwidth of matrix A small, the term ϕ_x is formulated as a one-sided derivative. In finite-difference form the equations are

$$\frac{p_P - p_S}{\Delta y} = \frac{1}{f}\frac{\phi_P - \phi_W}{\Delta x} + G, \qquad \phi_P = \frac{\nu}{h^2}\frac{p_A - 2p_P + p_B}{\Delta\theta^2}. \tag{B8}$$

At the surface corner point ($x = 0, \theta = 0$) the two conditions are Eqs. (A4a), expressed so that they do not involve exterior points,

$$p_{BB} - 4p_B + 3p_P = 0, \qquad \phi_{BB} - 4\phi_B + 3\phi_B = 0. \tag{B9}$$

At the bottom corner point ($x = 0, \theta = -1$), the two conditions are Eqs. (A4b) with $h_x = 0$. Thus, one of the conditions is just $\phi_\theta = 0$. With ϕ_θ expressed in a form that does not involve exterior points, this condition is

$$-\phi_{AA} + 4\phi_A - 3\phi_P = 0. \tag{B10}$$

The other condition is the expression for bottom drag, and requires that p is known at exterior points east of the coast. The coastal requirement $p_{xx} = 0$ allows these points to be eliminated, and the second bottom corner condition becomes

$$\frac{1}{\Delta x}\frac{\nu}{h}\left[\frac{-p_{NN} + 4p_N - 3p_P}{2\Delta\theta} - \frac{-p_{NNW} + 4p_{NW} - 3p_W}{2\Delta\theta}\right] = \gamma\frac{p_P - p_W}{\Delta x}. \tag{B11}$$

The reason that h_x must vanish at the coast is due entirely to this condition; without this assumption it would not be possible to eliminate exterior points.

The offshore boundary conditions (A4d) are written as one-sided derivatives, so that

$$p_P = p_E, \qquad \phi_P = \phi_E. \tag{B12}$$

The initial condition (A4e) is needed at the initial space-step to specify the value of p_S and p_{SA} in (B6) and (B8).

REFERENCES

Allen, J. S. 1973. Upwelling and coastal jets in a continuously stratified ocean. J. Phys. Oceanogr., *3,* 245–257.

—— 1980. Models of wind-driven currents on the continental shelf. Ann. Rev. Fluid Mech., *12,* 389–433.

Anderson, D. L. T. and A. E. Gill. 1975. Spin-up of a stratified ocean, with application to upwelling. Deep-Sea Res., *22,* 583–596.

Anderson, D. L. T. and P. D. Killworth. 1977. Spin-up of a stratified ocean with topography. Deep-Sea Res., *24,* 709–732.

Brockmann, C., E. Fahrbach, A. Huyer and R. L. Smith. 1980. The poleward undercurrent along the Peru coast: 5°–15°S. Deep-Sea Res., *217,* 847–856.

Csanady, G. T. 1978. The arrested topographic wave. J. Phys. Oceanogr., *8,* 47–62.

Forsythe, G. E. and C. B. Moler. 1967. Computer Solution of Linear Algebraic Systems, Prentice Hall, NJ, 148 pp.

Gill, A. E. and E. H. Schumann. 1974. The generation of long shelf waves by wind. J. Phys. Oceanogr., *4,* 83–90.

Hickey, B. M. 1979. The California Current system—hypotheses and facts. Prog. Oceanogr., *8,* 191–279.

Huthnance, J. M. 1981. Waves and currents near the continental shelf edge. Prog. Oceanogr., *10,* 193–226.

Kundu, P. J. and J. S. Allen. 1976. Some three-dimensional characteristics of low frequency current fluctuations near the Oregon coast. J. Phys. Oceanogr., *6,* 238–242.

McCreary, J. P. 1981. A linear stratified ocean model of the coastal undercurrent. Phil. Trans. R. Soc. Lond., A302, 385–413.

Miura, H. and N. Suginohara. 1980. Effects of bottom topography and density stratification on the formation of western boundary currents, Part 1. Wind-driven general circulation model. J. Oceanogr. Soc. Japan, *35,* 205–223.

Mooers, C. N. K., C. A. Collins and R. L. Smith. 1976. The dynamic structure of the frontal zone in the coastal upwelling region of Oregon. J. Phys. Oceanogr., *6,* 3–21.

Munk, W. H. 1950. On the wind-driven ocean circulation. J. Meteorol., *5,* 1–43.

Nelson, C. S. 1976. Wind stress and wind stress curl over the California coast. M.S. thesis, Naval Postgraduate School, Monterey, CA, 136 pp.

O'Brien, J. J., R. M. Clancy, A. J. Clarke, M. Crepon, R. Ellsburg, T. Grammelsrod, M. MacVean, L. P. Roed and J. D. Thompson. 1977. Upwelling in the ocean: two- and three-dimensional models of upper ocean dynamics and variability, *in* Modelling and Predicting the Upper Layers of the Ocean, Pergamon Press, NY, 178–228.

Pedlosky, J. 1974. On coastal jets and upwelling in bounded basins. J. Phys. Oceanogr., *4,* 3–18.

Philander, S. G. H. and J. -H. Yoon. 1982. Eastern boundary currents and coastal upwelling. J. Phys. Oceanogr., *12,* 862–879.

Suginohara, N. 1982. Coastal upwelling: Onshore-offshore circulation, equatorward coastal jet and poleward undercurrent over a continental shelf-slope. J. Phys. Oceanogr., *12,* 272–284.

Suginohara, N. and Y. Kitamura. 1984. Long-term coastal upwelling over continental shelf-slope. J. Phys. Oceanogr., *14,* 1095–1104.

Wang, D. -P. 1982. Development of a three-dimensional, limited-area (island) shelf circulation model. J. Phys. Oceanogr., *12,* 605–617.

Wang, D. -P. and C. N. K. Mooers. 1976. Coastal trapped waves in a continuously stratified ocean. J. Phys. Oceanogr., *6,* 853–863.

Received: *23 February, 1984;* revised: *24 October, 1984.*